Geophysical Research Letters

RESEARCH LETTER
10.1029/2023GL105689

Pressurizing Magma Within Heterogeneous Crust: A Case Study at the Socorro Magma Body, New Mexico, USA

Grant A. Block[1], Mousumi Roy[1], Emily Graves[2], and Ronni Grapenthin[2]

[1]Department of Physics and Astronomy, University of New Mexico, Albuquerque, NM, USA, [2]Geophysical Institute and Department of Geoscience, University of Alaska, Fairbanks, AK, USA

Key Points:

- InSAR confirms coeval subsidence and uplift (a so-called "sombrero" deformation pattern) persisted for >100 years at the Socorro Magma Body (SMB)
- A compliant region, modeled as a viscoelastic body surrounding a sill, is able to reproduce both the pattern and duration of deformation
- Viscoelastic deformation within a broad compliant region supports the presence of mush zones at SMB and other mid-crustal magma bodies

Supporting Information:

Supporting Information may be found in the online version of this article.

Correspondence to:

G. A. Block,
gblock@unm.edu

Citation:

Block, G. A., Roy, M., Graves, E., & Grapenthin, R. (2023). Pressurizing magma within heterogeneous crust: A case study at the Socorro magma body, New Mexico, USA. *Geophysical Research Letters*, *50*, e2023GL105689. https://doi.org/10.1029/2023GL105689

Received 7 AUG 2023
Accepted 7 OCT 2023

Abstract Surface deformation plays a key role in illuminating magma transport at active volcanoes, however, unambiguous separation of deep and shallow transport remains elusive. The Socorro Magma Body (SMB) lacks an upper crustal magma transport system, allowing us to link geodetic measurements with predictions of numerical models investigating rheologic heterogeneities and magma-mush interaction in the mid-/lower crust. New InSAR observations confirm that a pattern of central surface uplift surrounded by a region of subsidence (previously coined "sombrero" deformation) has persisted over >100 years at the SMB. Our models suggest this pattern may reflect the presence of a large (>100 km width), weaker-than-ambient, compliant region (CR) surrounding the mid-crustal magma body. Interactions between a pressurizing (e.g., due to melt injection and/or volatile exsolution) sill-like magma body and CR drive the sombrero pattern, depending on both viscoelastic relaxation and pressurization timescales, explaining its rare observation and transient nature.

Plain Language Summary Magma in the crust is transported and stored within magma bodies (regions that are mostly liquid magma) and "mush" (mostly solid crystals and some liquid magma). Mush zones are thought to be too viscous to be erupted but are likely to be weaker than the surrounding rock. To understand volcanic eruptions, it is important to understand the distribution of magma and mush, and their mutual interactions. Here we study these interactions in a mid-crustal magma body, the Soccorro Magma Body (SMB), that does not have a surface volcano. Surface deformation at the SMB helps us study magma-mush interaction, especially in the middle or lower crust. Previous surface deformation measurements at the SMB show "sombrero" deformation: a central area of uplift surrounded by a ring of subsidence. New satellite radar measurements are consistent with the previously reported pattern, confirming that this deformation remained remarkably constant through nearly 100 years. We suggest this is due to a large weak, mush region surrounding the SMB. Our computer models reproduce a long-lasting, consistent sombrero deformation pattern depending on mush properties as well as pressurization history of the magma body, and we suggest these factors may explain why this pattern is relatively rare.

1. Introduction

Long-lived active volcanic centers are the uppermost expression of a complex transcrustal transport system bringing magma from beneath and within the lithosphere to the surface (e.g., Cashman et al., 2017; Hildreth & Wilson, 2007). These systems comprise partially molten regions, thought to be a combination of crystal-poor magma bodies surrounded by crystal-rich "mush" zones near solidus (Cooper & Kent, 2014; Glazner et al., 2016; Jackson et al., 2018). Mush zones, where crystal volume fractions exceed 50%–60%, are thought to be deformable but not readily eruptible (e.g., Bachmann & Bergantz, 2008; A. Costa et al., 2009). Within them, the formation of crystal-poor (<50% crystals by volume) eruptible magma (e.g., Hughes et al., 2021) by heat and mass transfer is the subject of multidisciplinary exploration (e.g., Bergantz et al., 2015; F. Costa et al., 2020). Magma-mush interactions have been modeled as (visco)poroelastic coupling over length scales of intrusions (Alshembari et al., 2023; Liao et al., 2018, 2021; Mullet & Segall, 2022), or permeable flow and transport (Liu & Lee, 2021), possibly including the effects of volatiles (e.g., Parmigiani et al., 2014).

Mush zones in the upper crust are well documented at a number of active volcanic centers (e.g., Hamling et al., 2015), however, the role of mush in the mid-/lower crust is poorly understood (Annen et al., 2006; Magee et al., 2018; Maguire et al., 2022). For example, seismic observations at two large and dynamic mid-crustal magma bodies, the Socorro Magma Body (SMB) and the Altiplano-Puna Magma Body (APMB), suggest a broad

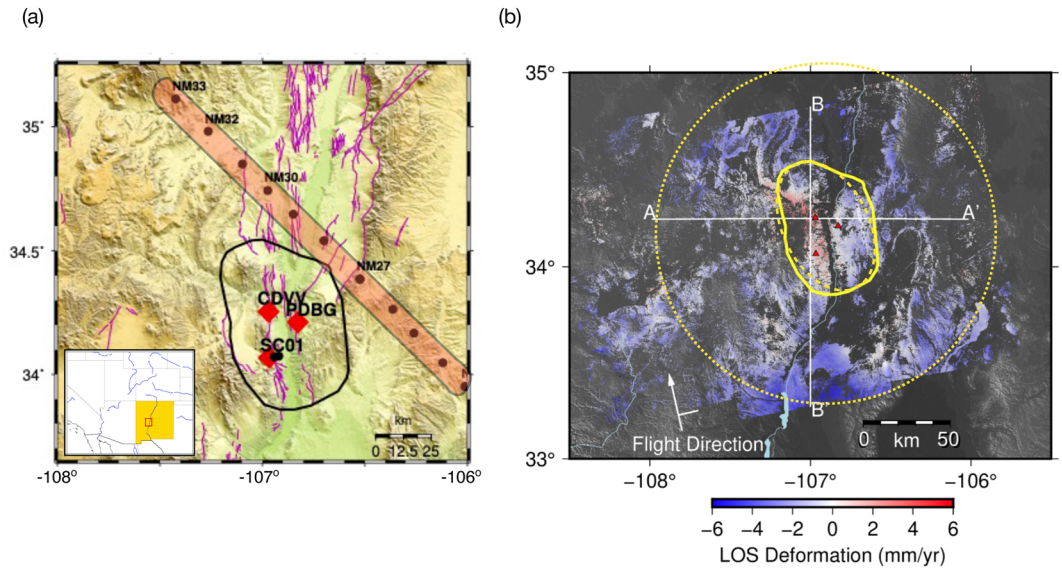

Figure 1. (a) Topographic relief map of the seismically derived extent of the Socorro Magma Body (SMB), New Mexico (Balch et al., 1997; Rinehart & Sanford, 1981), within southwestern North America (inset). Quaternary faults (magenta lines), three continuous GPS stations (red diamonds), and locations of the La Ristra seismic stations (black dots) (West et al., 2004) indicated for reference. The orange polygon outlines the NW-SE extent of low mid-crustal seismic wavespeeds (relative $V_s < -5\%$ at ≈20 km depth, from West et al. (2004). (b). InSAR measurements of the SMB spanning 01/07/2017 through 12/21/2021 showing the observed sombrero-style surface deformation. GPS stations (red) and the SMB outline (solid yellow) are as in (a). The yellow ellipse (long-dashes) outlines the pressure source and the larger yellow circle (short-dashes) shows the map-extent of the CR in the SMB-realistic model (Figure 5).

(>100 km wide; e.g., Figure 1a) region of anomalously low seismic wavespeeds in the mid-crust (Gao et al., 2004; Pritchard & Gregg, 2016; Ward et al., 2014; West et al., 2004; Wilson et al., 2005). These seismic anomalies coincide with volcanism (e.g., at the APMB, Long Valley, or Yellowstone) or elevated surface heatflow (e.g., Reiter et al., 2010), anomalous resistivity structure (e.g., Comeau et al., 2015), and anomalous seismicity (Hudson et al., 2022; Jay et al., 2012; Rinehart & Sanford, 1981; Sanford et al., 2002; Stankova et al., 2008), suggesting they are thermally/mechanically anomalous. While these regional mid-crustal seismic anomalies are consistent with the presence of melt (Ake & Sanford, 1988; Magee et al., 2018; Maguire et al., 2022), we lack an understanding of how magma and mush may be distributed within them and what role they play in the larger transcrustal magma transport system. For example, the APMB underlies numerous volcanoes (Gottsmann et al., 2017; Magee et al., 2018) and it is not clear how magma and mush are distributed within it. Thermal modeling of episodic melt injection suggests prolonged heating is necessary to generate long-lived mush zones (Annen et al., 2015; Blundy & Annen, 2016; Karakas et al., 2017). Such mush zones are likely weaker than the surrounding crust (Diener & Fagereng, 2014), but the implications of the resulting rheologic heterogeneity have not been fully considered in studies of surface deformation due to pressurizing mid-crustal magma bodies.

Inspired by regionally-extensive mid-crustal seismic anomalies, we use numerical models to study the role of spatial (horizontal and vertical) heterogeneity within the mid-crust in controlling the surface deformation response to mid-crustal magma pressurization. We are interested in the mechanical coupling between a mid-crustal compliant region (CR) and a pressurizing sill-like magma body. Separating surface deformation patterns due to mid-crustal magma injection and shallower magma dynamics proves difficult where the magma transport system extends to a volcanic system (e.g., Uturuncu Volcano, Long Valley, or Yellowstone) as upper crustal deformation obscures deeper processes (Biggs & Pritchard, 2017). The SMB (Figure 1), a large, seismically inferred, sill-like magma body at 19 km depth (diameter 50–70 km and thickness <1 km; Rinehart & Sanford, 1981; Balch et al., 1997; Fialko et al., 2001), does not have a volcanic expression. We exploit this lack of upper crustal magma transport at the SMB to directly connect geodetic observations to mid-crustal drivers of deformation.

Our starting point is a pattern of central uplift surrounded by subsidence, so-called "sombrero uplift" (coined by Fialko & Pearse, 2012), observed above both the SMB (Fialko & Pearse, 2012; Finnegan & Pritchard, 2009; Larsen et al., 1986; Pearse & Fialko, 2010) and the APMB at Uturuncu volcano (Fialko & Pearse, 2012; Gottsmann

et al., 2018; Henderson & Pritchard, 2017). For the APMB this deformation has been modeled as deformation that couples magma injection at depth with either deeper crustal mechanics (Fialko & Pearse, 2012; Henderson & Pritchard, 2017), or the dynamics of a shallow upper-crustal mush zone (Gottsmann et al., 2017). The SMB, however, lacks an upper crustal expression of the magma transport system motivating the question of how such a sombrero pattern might arise and what impact the presence of a CR may have.

A key finding of our study is that a mid-crustal CR surrounding the SMB leads to a spatial decoupling of surface deformation. Generally, vertical surface uplift directly above a pressurizing sill-like body (radius r_{source}) within a CR may be accompanied by surface subsidence of regions toward the edges of the CR ($r \gtrapprox 1.5 r_{source}$), providing an alternative mechanism for emergence of the sombrero pattern. The transient nature of the somberro pattern and its duration ($\Delta\tau_{som}$) is a strong function of the rheologic gradients within the CR and the pressure-time history within the sill, providing an explanation for its rare observation. Importantly, the surface expression of the deformation is controlled by the interplay of the pressurization timescale and the effective (viscoelastic) response timescale in the CR.

2. Deformation Observations at the Socorro Magma Body

At the SMB, the sombrero pattern of surface motion has been measured over nearly 100 years through leveling (Larsen et al., 1986) and Interferometric Synthetic Aperture Radar (InSAR) (Fialko et al., 2001; Pearse & Fialko, 2010). These observations, together with other geodetic measurements (Berglund et al., 2012; Larsen et al., 1986), suggest a maximum vertical uplift rate of ≈2–2.5 mm/yr.

We acquire Synthetic Aperture Radar (SAR) observations on ascending path 49 frame 107 (Figure 1b), collected by the European Space Agency's Sentinel-1 A/B mission (Torres et al., 2012), which we process with GMTSAR (Sandwell et al., 2011) to create 2 pass interferograms spanning January 2017 though December 2021. We create mean velocity stacks (Text S1 in Supporting Information S1) from individual interferograms which include December through January multi-year pairs by averaging the observed line-of-sight (LOS) deformation over the time interval of acquisition where observations are weighed by the time interval (e.g., Xiao et al., 2020). The resulting LOS velocity field (Figure 1b), aligned with prior observations (Fialko et al., 2001; Finnegan & Pritchard, 2009; Pearse & Fialko, 2010) to fit the magnitude of observations, reveals deformation overlying the SMB. From the average LOS deformation map (Figure 1b), we extract profiles for comparison to our SMB-specific finite-element model results (Figure 5c). We observe ≈3 mm/yr of peak LOS uplift within the SMB, with uplift limited to the central to western portion of the magma body. North-south and east-west profiles across the peak deformation illustrate the sombrero uplift over the magma body as described by Pearse and Fialko (2010). While residual topography impacts may bias the velocity field, we do not observe similar effects over other nearby topography.

Previous InSAR observations over the SMB report deformation rates of 2–3 mm/yr (Fialko et al., 2001; Finnegan & Pritchard, 2009; Pearse & Fialko, 2010), comparable to our observations during the duration of the SAR acquisitions. We observe a north-south elongated region of uplift, more consistent with Fialko et al. (2001) than the circular deformation shown by Finnegan and Pritchard (2009). Temporal changes in the InSAR-derived average LOS velocities over the SMB were presented in Finnegan and Pritchard (2009), therefore, variations in the shape of the region experiencing uplift during our study are not unprecedented.

This deformation signal is generally attributed to injection of magma in the mid-crust, however, many studies suggest it cannot be due to solely elastic effects (e.g., Fialko & Pearse, 2012; Fialko et al., 2001; Pearse & Fialko, 2010). Previous models of deformation at the SMB (Larsen et al., 1986; Fialko et al., 2001; Pearse & Fialko, 2010; Finnegan & Pritchard, 2009; A. Newman et al., 2001; A. V. Newman et al., 2006) do not explicitly consider material heterogeneity in a mid-crustal CR, the main target of our investigation.

3. Numerical Modeling Results

We present generic finite element models using PyLith (v2.2.2; Aagaard et al., 2019), to assess the role of a CR surrounding a sill-like pressure source in the mid-crust. We target the role of the CR and its manifestation in ground deformation (parameters and model details in Text S2, Table S1, and Figure S1 in Supporting Information S1). Each model comprises a background layered structure, with deformation driven by time-varying

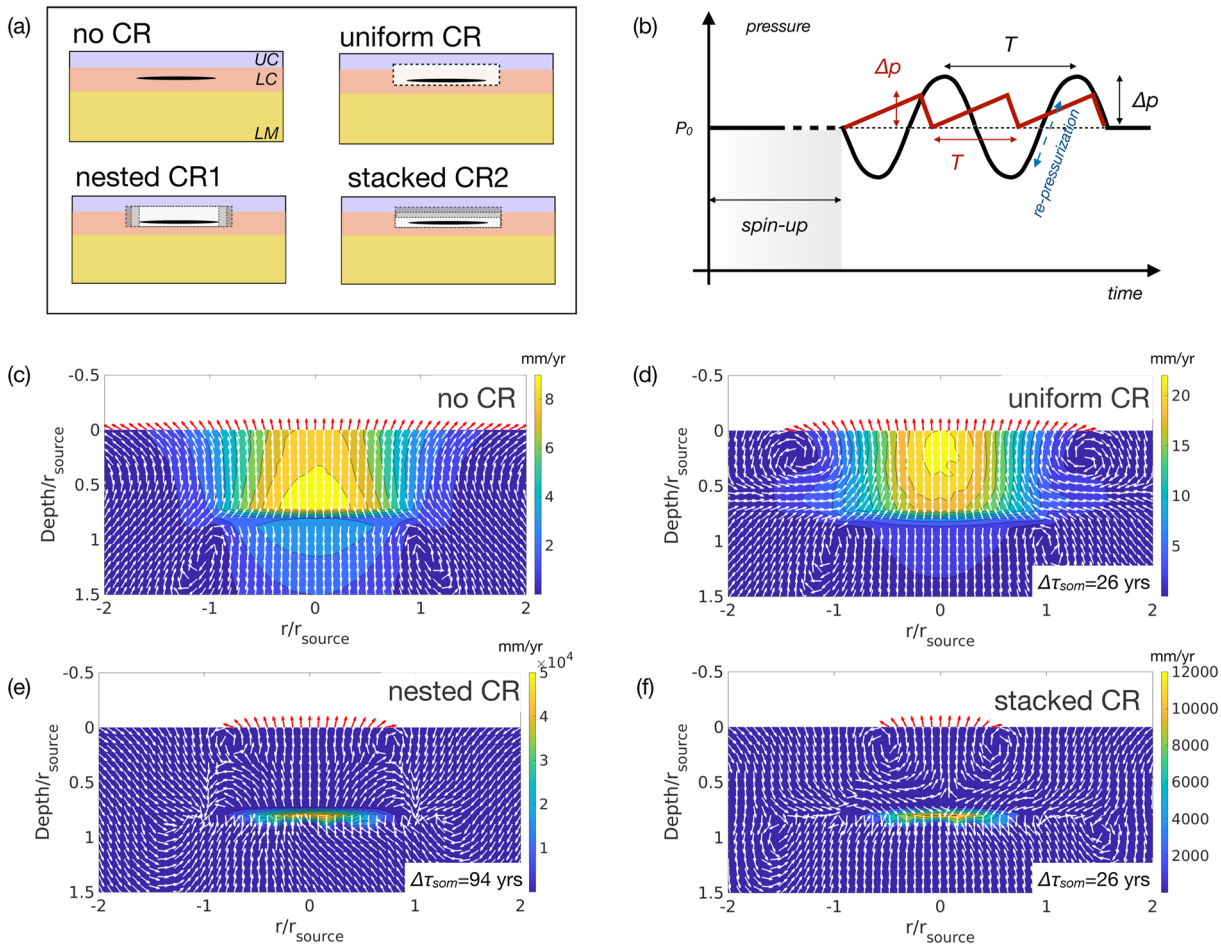

Figure 2. (a) Cross-section cartoons of generic models with variable CR. All models share a layered background rheology (UC = upper crust, LC = lower crust, LM = lithospheric mantle; see Text S2 in Supporting Information S1), within which a mid-crustal pressure source is embedded (black ellipse). The CR rheology is specified with a single viscosity (uniform CR) or with horizontal gradient in nested cylinders (nested CR) or vertical gradient in stacked cylinders (stacked CR). The nested CR viscosity increases radially and the stacked CR has viscosity increasing vertically. (b) After initial pressurization to a background pressure P_0, followed by a prescribed "spin-up" time at constant pressure, one of two periodic pressure functions is applied: a sinusoid with amplitude ΔP and period T (black), or sawtooth with pressure change ΔP and period T (red). The "re-pressurization" phase of a given pressure-time function refers to intervals with $dP/dt > 0$ as indicated (blue dashed arrows). (c)–(f) Cross sections illustrating spatially-varying velocity (arrows) for models with the same $r_{source} = 25$ km, $P_0 = 1$ MPa, $\Delta P = 500$ kPa and $T = 200$ years, (with sinusoidal pressurization), but with differing CR: (c) no CR, (d) a uniform CR, (e) nested CR, and (f) stacked CR. Velocity snapshots are shown halfway during the sombrero (d-f; durations indicated) or halfway through a pressure cycle (c). Arrows show velocity direction; red arrows indicate upward surface motions and color contours indicate velocity magnitude (mm/yr). Note the color bar range is different for each subplot.

pressurization of a mid-crustal sill (Figure 2b). We consider a suite of models, with and without a viscoelastic CR surrounding the sill, and explore the effects of varying CR structure (Figure 2a; Table S1 in Supporting Information S1).

A viscoelastic CR in the mid-crust (with lower viscosity than the ambient viscoelastic crust), leads to a phase-lag in surface deformation. When the sill within the CR undergoes pressurization, regions above its center and those to its edges (e.g., $r \geq 1.5r_{source}$) may be out of phase (demonstrated for vertical motions in Figure 3a and for horizontal motions in Figure S3 in Supporting Information S1). This is the essence of the sombrero signal (central uplift surrounded by an annular moat of subsidence), and we observe this pattern during the (re-)pressurization phase (Figure 2b), where the center begins to uplift while the edges are still subsiding due to viscoelastic relaxation of the CR. The sombrero pattern is only observed in the presence of a CR (Figure 3a); without it, surface velocities are in phase everywhere and have the same sign (Figure 3b).

When a CR exists, surface motions above the source (within $r/r_{source} \leq 1$) and outside it ($r/r_{source} \gtrapprox 1.5$) depend on: (a) rheologic gradients within the CR and (b) the applied pressurization history (Figures 3c–3f). Depending

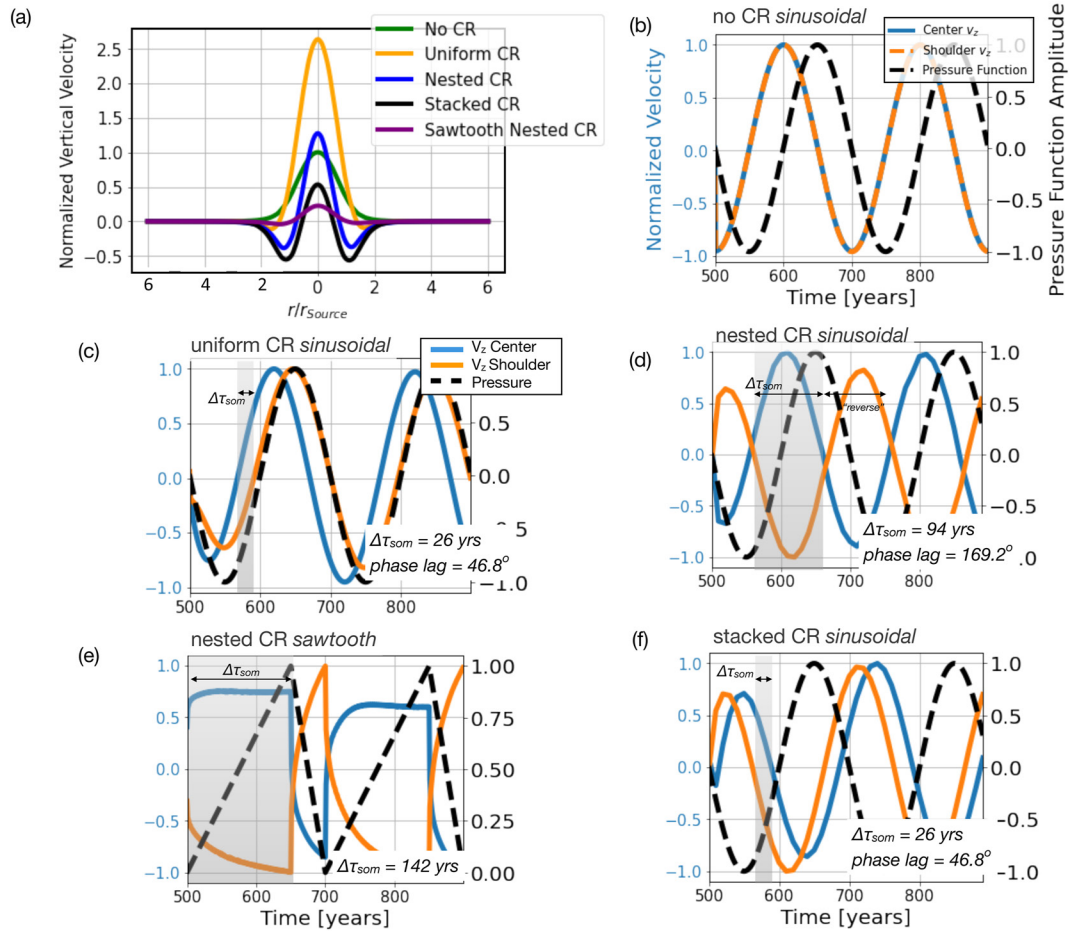

Figure 3. (a) Normalized vertical surface velocity, V_z, profiles (normalized relative to the maximum velocity of the no CR case), illustrating the role of the CR in the sombrero pattern of deformation in four models with varying CR; all with $P_0 = 1$ MPa, $\Delta P = 500$ kPa and $T = 200$ years. Each profile is shown at the same times as the corresponding velocity fields in Figures 2c–2f; see Figure S3 in Supporting Information S1 for corresponding radial motions. (b–d): Normalized surface uplift velocities at the center ($r = 0$ km, blue) and shoulder (defined as $r/r_{source} = 1.6$, orange), with normalized sinusoidal pressure-time variation (black dashed lines); y-axis labels for (c–f) are as indicated on (b). (b) No CR (corresponds to model in Figure 2c), (c) a uniform CR (model in Figure 2d), and (d) nested CR (model in Figure 2e). (e–f) Show decoupled center and shoulder velocities for the (e) nested CR and (f) stacked CR driven by pressurization functions as indicated.

on the gradient of viscosity within the CR, we observe a circulatory pattern of motion in the mid-crust (e.g., Figure 2d,e) and a phase lag between vertical surface velocities above the sill ("center") and outside of the source radius ("shoulder"; Figures 3c–3f; see also Figure S2 in Supporting Information S1). The time interval when vertical velocities at the center are positive and the shoulder regions are subsiding is the sombrero duration, $\Delta\tau_{som}$ (and vice versa, for a "reverse" sombrero, e.g., Figure 3d).

Spatial decoupling of the center and shoulder velocities during sombrero deformation depends on the rheologic gradient within the CR: comparing uniform CR model versus models with horizontal ("nested") and vertical ("stacked") viscosity gradients (Figure 2a). A larger CR viscosity gradient increases the phase lag compared to the uniform CR models (Figures S2b and S2d in Supporting Information S1), with systematically higher phase lags in the nested CR model than the stacked CR model (Figure S2 in Supporting Information S1). Horizontal viscosity gradients are, therefore, more important than vertical ones for controlling sombrero-style deformation.

In addition to rheologic gradients, the phase lag in surface velocities is strongly controlled by the pressure-time function. Sinusoidal pressure-time functions yield periodic motions where $\Delta\tau_{som}$ corresponds to a fixed (phase- and) time-lag for both the sombrero and the reverse sombrero (Figures 3c, 3d, and 3f). For sawtooth pressurization, however, the duration of the sombrero may greatly exceed that of the reverse pattern (Figure 3e). Nested CR

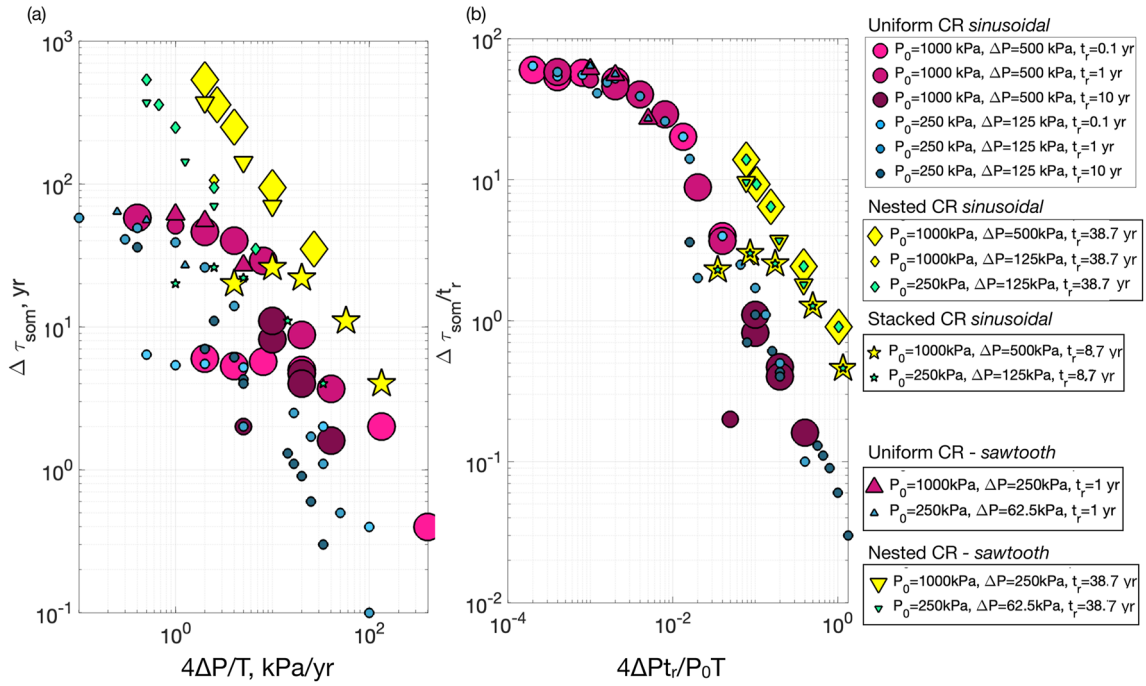

Figure 4. (a) Sombrero duration as a function of pressurization rate for the suite of models in this study. (b) Dimensionless sombrero duration (normalized by CR relaxation time) versus dimensionless pressurization rate (normalized by background pressure and CR relaxation time). In (a and b), we see a general trend of increasing sombrero duration with decreasing pressurization rate, up to a threshold. Nondimensionalization collapses all uniform CR runs into a single trend, and likewise with the nested CR and stacked CR models. To normalize nested CR and stacked CR runs, t_r was found by volumetrically averaging the relaxation times within the CR.

models driven by sawtooth pressurization (Figure 3e) exhibit near-constant surface velocities during a sombrero event.

Decreasing the pressurization rate (e.g., $dP/dt \approx 4\Delta P/T$ for the sinusoidal function) leads to increased sombrero duration, $\Delta\tau_{som}$ (Figure 4). The sombrero duration $\Delta\tau_{som}$ for a given $\Delta P/T$ increases with the ambient background pressure, P_0, and decreases with relaxation time t_r (Figure 4a). For the uniform CR, the relation between $\Delta\tau_{som}$ and $\Delta P/T$ collapses into a single trend when the duration is normalized by the uniform relaxation time within the CR, t_r, and the pressurization rate is normalized by P_0/t_r (Figure 4b). Nested and stacked CR runs also collapse onto similar trends showing an increase in $\Delta\tau_{som}$ at low $\Delta Pt_r/P_0T$, with systematically higher sombrero durations compared to the uniform CR models at the same dimensionless pressurization rate (Figure 4b). (We use a volumetrically-averaged relaxation time to nondimensionalize in non-uniform CRs). For the uniform and stacked CR models, there is a transition at low $\Delta Pt_r/P_0T$ at which the sombrero duration is not as sensitive to the pressurization rate. The slope of the trend is similar for nested CR models, but without a similar observed transition at low rates. (Reaching a dimensionless pressurization rate of $\Delta Pt_r/P_0T = 10^{-2}$ is computationally expensive for the nested and stacked CR models due to the large volumetrically-averaged t_r.) The uniform and stacked CR models clearly reach a threshold at which $\Delta\tau_{som}$ appears to be nearly independent of $\Delta Pt_r/P_0T$, suggesting the threshold depends on intra-CR rheology ($\Delta Pt_r/P_0T \approx 10^{-2}$ for uniform CR and 10^{-1} for stacked CR; Figure 4b). Models with the same pressurization rate but different pressure-time functions show little variation in sombrero duration, demonstrating that the primary controlling factors for sombrero duration are the pressurization rate and model geometry, and not pressure-time history (Figure 4).

4. Discussion

While idealized, the generic models above demonstrate that a weaker-than-ambient CR surrounding a (de-)pressurizing sill can decouple surface deformation directly above the sill from points farther away. A key finding is that, during pressurization, locations vertically above the sill may be uplifting while those outside the surface projection of the sill may be subsiding, creating a sombrero pattern (Figure 3). (The pattern may be reversed when transitioning to a period of de-pressurization.) This phase lag in the surface deformation pattern

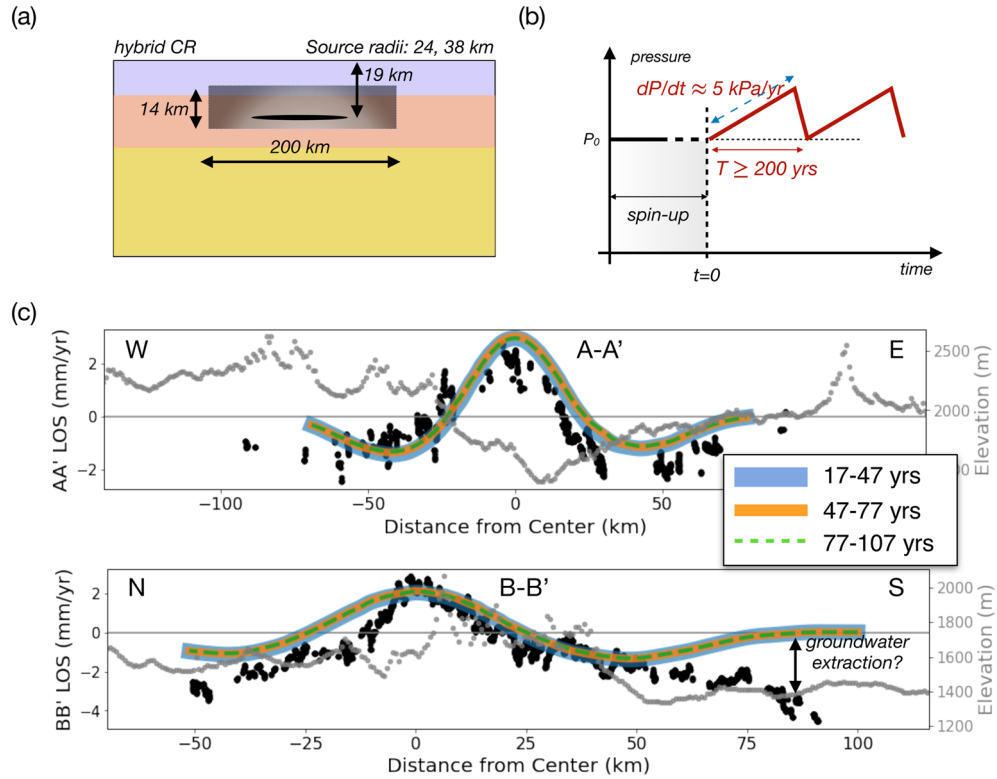

Figure 5. Summary of SMB-specific ellipsoidal source/hybrid CR model (Table S1 in Supporting Information S1) and results. (a) Cartoon schematic illustrating the CR (200 km diameter), with both horizontal and vertical gradients in t_r (represented by the shading moving away from the pressure source (black); Table S1 in Supporting Information S1). (b) Sketch of pressure-time function, with constant pressurization at $dP/dt \approx 5$ kPa/yr, leading to a nearly stationary sombrero pattern over $\Delta t_{som} > 100$ years (sawtooth period $T \geq 200$ years). (c) Predicted surface velocity profiles (solid and dashed lines) extracted along lines A-A′ and B-B′ in Figure 1b, projected onto the LOS and averaged over 30 years windows as indicated ($t = 0$ is defined at the beginning of the sawtooth function in (b)). Lines extracted from the model are offset by 10.0 km west and 0.5 km north and rotated by −22.55°. InSAR LOS velocities along profiles A-A′ and B-B′ (black dots) and topography (light gray dots) are plotted for comparison. The data were converted from degrees to km with the factor 1° ≈ 93 km. The misfit at the southern end of the B-B′ profile is likely due to groundwater extraction from local agricultural activity.

depends on the presence of the CR, but the duration of the sombrero depends primarily on pressurization rate: increasing with decreasing pressurization rate, up to a threshold (Figure 4). Strong viscosity gradients paired with asymmetric pressurization lead to long sombrero durations with nearly steady ground motions (Figures 3e and 4b). Crucially, a long period of re-pressurization (with roughly constant dP/dt) followed by a sudden decrease in pressure results in a sombrero that lasts longer than the reverse-sombrero, with slowly-varying surface velocities during the sombrero (Figure 3d). Although we lack contraints on SMB sill pressures, rheologic properties of anatexites suggest that the bulk strength of partially-molten rocks in the middle or lower crust range from ≤1 to 5 MPa during cycles of melt production and drainage (Diener & Fagereng, 2014). The range of background pressures, P_0, and pressure changes ΔP, in our models (Figure 4) is consistent with expectations for weakened partially molten crustal mineralogies (Diener & Fagereng, 2014).

We now present an SMB-specific model constrained by seismic and geodetic observations discussed above: (a) a sill-like body at ≈19 km depth, elliptical in mapview, surrounded by anomalously low V_s in the mid-crust (Balch et al., 1997; Rinehart & Sanford, 1981; West et al., 2004, Figure 1a); and (b) a long-lived ($\Delta\tau_{som} \geq 100$ years) sombrero pattern of deformation, with nearly constant surface motions (Fialko et al., 2001; Finnegan & Pritchard, 2009; Pearse & Fialko, 2010; Larsen et al., 1986, Figure 1). Assuming that the V_s anomaly ≤−5% at ≈20 km depth region in West et al. (2004) is a proxy for a weaker-than-ambient CR (dashed yellow circle in Figure 1b), we specify horizontal and vertical gradients in CR viscosity (see Table S1 in Supporting Information S1). The 200 km diameter of the hybrid CR follows the extent of the low-velocity mid-crustal V_s anomaly and the sill-like ellipsoidal source has thickness 1 km and mapview radii of 24 and 38 km (Figure 5a). With this

geophysically-informed SMB-model, we explore the background pressure P_0 needed to match the amplitude of the InSAR LOS observations and the pressurization rate dP/dt needed to generate a long-lived (>100 years) sombrero pattern.

We find that a sill pressurized to a background pressure of $P_0 = 1.0$ MPa, with a constant pressure increase of $dP/dt = 4\Delta P/T = 5$ kPa/yr (implemented as a sawtooth pressure-time function with $\Delta P = 250$ kPa and $T = 200$ years; Figure 5b), produces a reasonable fit to the InSAR observations (A-A′ and B-B′ in Figure 5c). The modeled sombrero duration of $\Delta\tau_{som} = 148$ years is characterized by persistent, nearly steady surface motions for over 100 years, comparable to long-term observations at the SMB (Figure 5c). The width of the modeled deformation depends on the seismically-constrained geometry, and no further adjustment was used to fit the width of the surface pattern in Figure 5c.

The inferred pressurization rate of $dP/dt \approx 5$ kPa/yr (comparable to Pearse & Fialko, 2010) may be interpreted as due to injection of magma, or to pressurization due to volatile degassing. If driven by magma injection alone, we infer a volumetric rate $dV/dt = \beta V_0(dP/dt)$ where β is the magma compressibility and V_0 is an initial volume. Compressibility of a gas-poor, basaltic magma at 19 km depth is likely lower than compressibility above 10 km depth (e.g., $\beta \approx 0.4 - 2 \times 10^{-10}$ Pa^{-1}; Rivalta and Segall (2008)), so $\beta = 0.4 \times 10^{-10}$ Pa^{-1} is a reasonable upper bound. Following pressurization to $P_0 \approx 1$ MPa, the initial volume of the ellipsoidal source (Table S1 in Supporting Information S1) is $\approx 1{,}940$ km^3, so $dV/dt \approx 3.88 \times 10^{-4}$ km^3/yr. On the other hand, if the source of pressurization includes exsolved volatiles, this inferred volumetric injection rate is likely an overestimate. A dry ($\leq$0.2 wt % H_2O) basaltic magma (e.g., expected in a rift-setting) with $\geq$4,000 ppm CO_2 at $\geq$1,000°C is likely to reach saturation at pressures above 500 MPa, comparable to conditions at 19 km depth within the Rio Grande Rift. We lack direct constraints on the CO_2 content of the SMB, however, mantle xenoliths from the nearby Rio Puerco and Kilbourne Hole Volcanic Fields have undergone metasomatism by carbonatitic fluids (Harvey et al., 2012; Porreca & Selverstone, 2006), suggesting that CO_2-rich fluids may be abundant in the SMB. Therefore, the inferred pressurization above may be due to a combination of gas exsolution together with magma injection, but we lack constraints on the relative roles of these processes.

Observations at the APMB span a shorter timeframe than the SMB, and suggest a peak uplift rate at Uturuncu Volcano of ≈0.5–1 cm/yr (Fialko & Pearse, 2012; Gottsmann et al., 2018; Henderson & Pritchard, 2017). Here, 50 years of geodetic observations suggest transient sombrero deformation (Eiden et al., 2023; Fialko & Pearse, 2012; Gottsmann et al., 2018), and our models provide an explanation for this transience. The inferred pressurization rate at the SMB (≈5 kPa/yr) is smaller than modeled beneath Uturuncu if all of the deformation is ascribed to upper crustal processes (Gottsmann et al., 2017). As we have demonstrated, for a given pressurization rate the duration of the sombrero pattern is controlled by decoupling between surface motions within $r < 1.5r_{source}$ and $r \geq 1.5r_{source}$, and this decoupling and phase lag depends on intra-CR viscosity gradients (Figure S2 in Supporting Information S1). Specifically, sombrero durations will be smaller (and therefore manifest their transience over shorter timescales) if the mid-crustal CR is uniform in rheology versus if it has significant rheologic gradients within it (Figure 4; S2). Our models raise the possibility that at least part of the transient sombrero pattern in the APMB may indeed be attributed to lateral heterogeneity in the mid-crust, with perhaps a more rheologically uniform CR than in the SMB.

While these results make a compelling case for the role of a weaker-than-ambient CR in the SMB geodetic signal, our models cannot differentiate between thermal weakening and the presence of mush within the CR. Thermoelastic effects have been inferred for driving deformation at active volcanoes (Furuya, 2005; Masterlark & Lu, 2004; Wang & Aoki, 2019). A simple inversion for thermoelastic drivers requires both heating and cooling sources deeper than the SMB (see Text S3 in Supporting Information S1). We suggest therefore that thermoelasticity is unlikely to be a primary driver of surface uplift in the region. Additionally, we acknowledge important complexities are ignored in our models, for example, near-surface hydrology and groundwater extraction (likely due to agriculture is evident at the southern end of profile B-B′ in Figure 5c, which crosses from the Socorro Basin into the Jornada del Muerto Basin). We also ignore extensional stress and material heterogeneity associated with the Rio Grande Rift. In future work, we hope to include heat transfer and poro(visco)-elastic effects to more fully explore CR heterogeneity and implications for magma-mush interactions. During time-variable pressurization in the sill, as magma is either sourced from deeper levels or drained from a mush, we might expect time-dependent rheology in the CR as explored in Liao et al. (2021), Liao et al. (2018), Mullet and Segall (2022), and Alshembari et al. (2023). These studies explore interactions in a single melt injection/withdrawal event, however, our models

highlight the importance of cyclic pressure-time variations, especially when a CR is present, in decoupled surface deformation. As shown by Liao et al. (2021), two important time scales for controlling stress transfer and surface deformation include a short time scale driven by poroelastic diffusion, and a longer viscoelastic relaxation time scale. Indeed, the fast depressurization in the sawtooth function may be a proxy for porous diffusion of magma into the surrounding CR mush zone, causing depressurization at a significantly faster rate than allowed by viscous relaxation. Over longer timescales, however, poroviscoelastic effects may be less important than the viscous relaxation behavior captured in our models (Text S3 in Supporting Information S1). Specifically, viscous creep within a weaker-than-ambient mid-crustal CR (e.g., a regionally-extensive partial melt-rich mush) and intra-CR rheologic gradients drive transient surface deformations as seen in the sombrero pattern.

Data Availability Statement

All PyLith input files and InSAR data will be made available at the following github repository: https://github.com/Grant-Block/SMB_FiniteElementModels.git and Zenodo (Block, 2023). The PyLith software is freely available at (Aagaard et al., 2019).

Acknowledgments
GB and MR thank: the UNM Center for Advanced Research Computing, supported in part by the National Science Foundation, for resources used in this work; Eric Lindsey for fruitful InSAR discussions; and David Wilson and Mike West for information regarding the La Ristra seismic experiment. MR thanks Emmanuel Codillo for discussions on the magma saturation pressures during the CIDER 2023 workshop. This work was completed while GB was partly supported by NSF EAR-2120812; GB also thanks the CONVERSE network for discussions which helped inform and contextualize this project. EG and RG acknowledge NASA funding through LNIP 80NSSC20K0073. Copernicus Sentinel data 2016–2020. Retrieved from ASF DAAC, processed by ESA.

References

Aagaard, B., Knepley, M., & Williams, C. (2019). Pylith v2.2.2 [Software]. Zenodo. https://doi.org/10.5281/zenodo.3269486

Ake, J., & Sanford, A. (1988). New evidence for the existence and internal structure of a thin layer of magma at mid-crustal depths near Socorro, New Mexico. *Bulletin of the Seismological Society of America*, *78*, 1335–1359. https://doi.org/10.1785/BSSA0780031335

Alshembari, R., Hickey, J., Williamson, B. J., & Cashman, K. (2023). Unveiling the rheological control of magmatic systems on volcano deformation: The interplay of poroviscoelastic magma-mush and thermo-viscoelastic crust. *Journal of Geophysical Research: Solid Earth*, *128*(7), e2023JB026625. https://doi.org/10.1029/2023JB026625

Annen, C., Blundy, J. D., Leuthold, J., & Sparks, R. S. J. (2015). Construction and evolution of igneous bodies: Towards an integrated perspective of crustal magmatism. *Lithos*, *230*, 206–221. https://doi.org/10.1016/j.lithos.2015.05.008

Annen, C., Blundy, J. D., & Sparks, R. S. J. (2006). The genesis of intermediate and silicic magmas in deep crustal hot zones. *Journal of Petrology*, *47*(3), 505–539. https://doi.org/10.1093/petrology/egi084

Bachmann, O., & Bergantz, G. (2008). The magma reservoirs that feed supereruptions. *Elements*, *4*(1), 17–21. https://doi.org/10.2113/GSELEMENTS.4.1.17

Balch, R. S., Hartse, H. E., Sanford, A. R., & wan Lin, K. (1997). A new map of the geographic extent of the Socorro mid-crustal magma body. *Bulletin of the Seismological Society of America*, *87*(1), 174–182. https://doi.org/10.1785/bssa0870010174

Bergantz, G. W., Schleicher, J. M., & Burgisser, A. (2015). Open-system dynamics and mixing in magma mushes. *Nature Geoscience*, *8*(10), 793–796. https://doi.org/10.1038/ngeo2534

Berglund, H. T., Sheehan, A. F., Murray, M. H., Roy, M., Lowry, A. R., Nerem, R. S., & Blume, F. (2012). Distributed deformation across the Rio Grande Rift, Great Plains, and Colorado plateau. *Geology*, *40*(1), 23–26. https://doi.org/10.1130/G32418.1

Biggs, J., & Pritchard, M. E. (2017). Global Volcano monitoring: What does it mean when volcanoes deform? *Elements*, *13*(1), 17–22. https://doi.org/10.2113/gselements.13.1.17

Block, G. (2023). Grant-Block/SMB_FiniteElementModels: SMBFiniteElement models [Software]. Zenodo. https://doi.org/10.5281/zenodo.8364972

Blundy, J. D., & Annen, C. J. (2016). Crustal magmatic systems from the perspective of heat transfer. *Elements*, *12*(2), 115–120. https://doi.org/10.2113/gselements.12.2.115

Cashman, K. V., Sparks, R. S. J., & Blundy, J. D. (2017). Vertically extensive and unstable magmatic systems: A unified view of igneous processes. *Science*, *355*(6331), 1280. https://doi.org/10.1126/science.aag3055

Comeau, M. J., Unsworth, M. J., Ticona, F., & Sunagua, M. (2015). Magnetotelluric images of magma distribution beneath volcan Uturuncu, Bolivia: Implications for magma dynamics. *Geology*, *34*(3), 243–246. https://doi.org/10.1130/G36258.1

Cooper, K. M., & Kent, A. J. R. (2014). Rapid remobilization of magmatic crystals kept in cold storage. *Nature*, *506*(7489), 480–483. https://doi.org/10.1038/nature12991

Costa, A., Caricchi, L., & Bagdassarov, N. (2009). A model for the rheology of particle-bearing suspensions and partially molten. *Geochemistry, Geophysics, Geosystems*, *10*, Q03010. https://doi.org/10.1029/2008GC002138

Costa, F., Shea, T., & Ubide, T. (2020). Diffusion chronometry and the timescales of magmatic processes. *Nature Reviews Earth & Environment*, *1*(4), 201–214. https://doi.org/10.1038/s43017-020-0038-x

Diener, J. F. A., & Fagereng, Å. (2014). The influence of melting and melt drainage on crustal rheology during orogenesis. *Journal of Geophysical Research: Solid Earth*, *119*(8), 6193–6210. https://doi.org/10.1002/2014JB011088

Eiden, E., MacQueen, P., Henderson, S., & Pritchard, M. E. (2023). Multiple spatial and temporal scales of deformation from geodetic monitoring point to active transcrustal magma system at Uturuncu volcano, Bolivia. *Geosphere*, *19*(X), 1–13. https://doi.org/10.1130/GES02520.1

Fialko, Y., & Pearse, J. (2012). Sombrero uplift above the Altiplano-Puna magma body: Evidence of a ballooning mid-crustal diapir. *Science*, *338*(6104), 250–252. https://doi.org/10.1126/science.1226358

Fialko, Y., Simons, M., & Khazan, Y. (2001). Finite source modelling of magmatic unrest in Socorro, New Mexico, and long valley, California. *Geophysical Journal International*, *146*(1), 191–200. https://doi.org/10.1046/j.1365-246X.2001.00453.x

Finnegan, N., & Pritchard, M. (2009). Magnitude and duration of surface uplift above the Socorro magma body. *Geology*, *37*(3), 231–234. https://doi.org/10.1130/G25132A.1

Furuya, M. (2005). Quasi-static thermoelastic deformation in an elastic half-space: Theory and application to InSAR observations at Izu-Oshima volcano, Japan. *Geophysical Journal International*, *161*(1), 230–242. https://doi.org/10.1111/j.1365-246x.2005.02610.x

Gao, W., Grand, S., Baldridge, W. S., Wilson, D., West, M., Ni, J., & Aster, R. (2004). Upper mantle convection beneath the central Rio Grande Rift imaged by P and S wave tomography. *Journal of Geophysical Research*, *109*(B3), B03305. https://doi.org/10.1029/2003JB002743

Glazner, A., Bartley, J., & Coleman, D. (2016). We need a new definition for "magma". *Eos*, *97*. https://doi.org/10.1029/2016EO059741
Gottsmann, J., Blundy, J., Henderson, S., Pritchard, M., & Sparks, R. (2017). Thermomechanical modeling of the Altiplano-Puna deformation anomaly: Multiparameter insights into magma mush reorganization. *Geosphere*, *13*(4), 1–24. https://doi.org/10.1130/GES01420.1
Gottsmann, J., del Potro, R., & Muller, C. (2018). 50 years of steady ground deformation in the Altiplano-Puna region of southern Bolivia. *Geosphere*, *14*(1), 65–73. https://doi.org/10.1130/GES01570.1
Hamling, I. J., Hreinsdottir, S., & Fournier, N. (2015). The ups and downs of the TVZ: Geodetic observations of deformation around the Taupo volcanic zone, New Zealand. *Journal of Geophysical Research: Solid Earth*, *120*(6), 4667–4679. https://doi.org/10.1002/2015JB012125
Harvey, J., Yoshikawa, M., Hammond, S. J., & Burton, K. W. (2012). Deciphering the trace element characteristics in Kilbourne Hole peridotite xenoliths: Melt-rock interaction and metasomatism beneath the Rio Grande Rift, SW USA. *Journal of Petrology*, *53*(8), 1709–1742. https://doi.org/10.1093/petrology/egs030
Henderson, S. T., & Pritchard, M. E. (2017). Time-dependent deformation of Uturuncu volcano, Bolivia, constrained by GPS and InSAR measurements and implications for source models. *Geosphere*, *13*(6), 1834–1854. https://doi.org/10.1130/GES01203.1
Hildreth, W., & Wilson, C. J. N. (2007). Compositional zoning of the bishop tuff. *Journal of Petrology*, *48*(5), 951–999. https://doi.org/10.1093/petrology/egm007
Hudson, T. S., Kendall, J.-M., Pritchard, M. E., Blundy, J. D., & Gottsmann, J. H. (2022). From slab to surface: Earthquake evidence for fluid migration at Uturuncu volcano, Bolivia. *Earth and Planetary Science Letters*, *577*, 117268. https://doi.org/10.1016/j.epsl.2021.117268
Hughes, G. E., Petrone, C. M., Downes, H., Varley, N. R., & Hammond, S. J. (2021). Mush remobilisation and mafic recharge: A study of the crystal cargo of the 2013–17 eruption at volcán de colima, Mexico. *Journal of Volcanology and Geothermal Research*, *416*, 107296. https://doi.org/10.1016/j.jvolgeores.2021.107296
Jackson, M. D., Blundy, J., & Sparks, R. S. J. (2018). Chemical differentiation, cold storage and remobilization of magma in the Earth's crust. *Nature*, *564*(7736), 405–409. https://doi.org/10.1038/s41586-018-0746-2
Jay, J. A., Pritchard, M. E., West, M. E., Christensen, D., Haney, M., Minaya, E., et al. (2012). Shallow seismicity, triggered seismicity, and ambient noise tomography at the long-dormant Uturuncu volcano, Bolivia. https://doi.org/10.1007/s00445-011-0568-7
Karakas, O., Degruyter, W., Bachmann, O., & Dufek, J. (2017). Lifetime and size of shallow magma bodies controlled by crustal-scale magmatism. *Nature Geoscience*, *10*(6), 446–450. https://doi.org/10.1038/ngeo2959
Larsen, S., Reilinger, R., & Brown, L. (1986). Evidence of ongoing crustal deformation related to magmatic activity near Socorro, New Mexico. *Journal of Geophysical Research*, *91*(B6), 6283–6292. https://doi.org/10.1029/JB091iB06p06283
Liao, Y., Soule, S. A., & Jones, M. (2018). On the mechanical effects of poroelastic crystal mush in classical magma chamber models. *Journal of Geophysical Research*, *123*(11), 9376–9406. https://doi.org/10.1029/2018JB015985
Liao, Y., Soule, S. A., Jones, M., & Le Mével, H. (2021). The mechanical response of a magma chamber with poroviscoelastic crystal mush. *Journal of Geophysical Research*, *126*(4), e2020JB019395. https://doi.org/10.1029/2020JB019395
Liu, B., & Lee, C.-T. (2021). Fast melt expulsion from crystal-rich mushes via induced anisotropic permeability. *Earth and Planetary Science Letters*, *571*, 117113. https://doi.org/10.1016/j.epsl.2021.117113
Magee, C., Stevenson, C. T., Ebmeier, S. K., Keir, D., Hammond, J. O., Gottsmann, J. H., et al. (2018). Magma plumbing systems: A geophysical perspective. *Journal of Petrology*, *59*(6), 1217–1251. https://doi.org/10.1093/petrology/egy064
Maguire, R., Schmandt, B., Li, J., Jiang, C., Li, G., Wilgus, J., & Chen, M. (2022). Magma accumulation at depths of prior rhyolite storage beneath Yellowstone caldera. *Science*, *378*(6623), 1001–1004. https://doi.org/10.1126/science.ade0347
Masterlark, T., & Lu, Z. (2004). Transient volcano deformation sources imaged with interferometric synthetic aperture radar: Application to Seguam Island, Alaska. *Journal of Geophysical Research*, *109*(B1), B01401. https://doi.org/10.1029/2003jb002568
Mullet, B., & Segall, P. (2022). The surface deformation signature of a transcrustal, crystal mush-dominant magma system. *Journal of Geophysical Research*, *127*(5), e2022JB024178. https://doi.org/10.1029/2022JB024178
Newman, A., Dixon, T. H., Ofoegbu, G., & Dixon, J. E. (2001). Geodetic and seismic constraints on recent activity at Long Valley caldera, California: Evidence for viscoelastic rheology. *Journal of Volcanology and Geothermal Research*, *105*(3), 183–206. https://doi.org/10.1016/S0377-0273(00)00255-9
Newman, A. V., Dixon, T. H., & Gourmelen, N. (2006). A four-dimensional viscoelastic deformation model for long valley caldera, California, between 1995 and 2000. *Journal of Volcanology and Geothermal Research*, *150*(1–3), 244–269. https://doi.org/10.1016/j.jvolgeores.2005.07.017
Parmigiani, A., Huber, C., & Bachmann, O. (2014). Mush microphysics and the reactivation of crystal-rich magma reservoirs. *Journal of Geophysical Research*, *119*(8), 6308–6322. https://doi.org/10.1002/2014JB011124
Pearse, J., & Fialko, Y. (2010). Mechanics of active magmatic intraplating in the Rio Grande Rift near Socorro, New Mexico. *Journal of Geophysical Research*, *115*(B7), B07413. https://doi.org/10.1029/2009JB006592
Porreca, C., Selverstone, J., & Samuels, K. (2006). Pyroxenite xenoliths from the Rio Puerco volcanic field, New Mexico: Melt metasomatism at the margin of the Rio Grande Rift. *Geosphere*, *2*(7), 333–351. https://doi.org/10.1130/ges00058.1
Pritchard, M. E., & Gregg, P. M. (2016). Geophysical evidence for silicic crustal melt in the continents: Where, what kind, and how much? *Elements*, *12*(2), 121–127. https://doi.org/10.2113/gselements.12.2.121
Reiter, M., Chamberlin, R. M., & Love, D. W. (2010). New data reflect on the thermal antiquity of the Socorro magma body locale, Rio Grande Rift, New Mexico. *Lithosphere*, *2*(6), 447–453. https://doi.org/10.1130/L115.1
Rinehart, E. J., & Sanford, A. R. (1981). Upper crustal structure of the Rio Grande Rift near Socorro, New Mexico, from inversion of microearthquake s-wave reflections. *Bulletin of the Seismological Society of America*, *71*(2), 437–450. https://doi.org/10.1785/BSSA0710020437
Rivalta, E., & Segall, P. (2008). Magma compressibility and the missing source for some dike intrusions. *Geophysical Research Letters*, *35*(4), L04306. https://doi.org/10.1029/2007gl032521
Sandwell, D., Mellors, R., Tong, X., Wei, M., & Wessel, P. (2011). Open radar interferometry software for mapping surface deformation. *Eos, Transactions American Geophysical Union*, *92*(28), 1090004. LLNL-TR-481284. https://doi.org/10.1029/2011EO280002
Sanford, A., Lin, K., Tsai, I., & Jacksha, L. (2002). Earthquake catalogs for New Mexico and bordering areas: 1869–1998.
Stankova, J., Bilek, S. L., Rowe, C. A., & Aster, R. C. (2008). Characteristics of the October 2005 microearthquake swarm and reactivation of similar event seismic swarms over decadal time periods near Socorro, New Mexico. *Bulletin of the Seismological Society of America*, *98*(1), 93–105. https://doi.org/10.1785/0120070108
Torres, R., Snoeij, P., Geudtner, D., Bibby, D., Davidson, M., Attema, E. e. a., et al. (2012). Gmes sentinel-1 mission. *Remote Sensing of Environment*, *120*, 9–24. https://doi.org/10.1016/j.rse.2011.05.028
Wang, X., & Aoki, Y. (2019). Posteruptive thermoelastic deflation of intruded magma in Usu volcano, Japan, 1992–2017. *Journal of Geophysical Research: Solid Earth*, *124*(1), 335–357. https://doi.org/10.1029/2018jb016729

Ward, K. M., Zandt, G., Beck, S. L., Christensen, D. H., & McFarlin, H. (2014). Seismic imaging of the magmatic underpinnings beneath the Altiplano-Puna volcanic complex from the joint inversion of surface wave dispersion and receiver functions. *Earth and Planetary Science Letters*, *404*, 43–53. https://doi.org/10.1016/j.epsl.2014.07.022

West, M., Ni, J., Baldridge, W., Wilson, D., Aster, R., Gao, W., & Grand, S. (2004). Crust and upper mantle shear-wave structure of the southwest United States: Implications for rifting and support for high elevation. *Journal of Geophysical Research*, *109*(B3), B03309. https://doi.org/10.1029/2003JB002575

Wilson, D., Aster, R., West, M., Ni, J., Grand, S., Gao, W., et al. (2005). Lithospheric structure of the Rio Grande Rift. *Nature*, *433*(7028), 851–855. https://doi.org/10.1038/nature03297

Xiao, R., Yu, C., Zhenhong, L., Song, C., & He, X. (2020). General survey of large-scale land subsidence by GACOS-corrected InSAR stacking: Case study in North China plain. In *Proceedings of the International Association of Hydrological Sciences* (Vol. 382, pp. 213–218). https://doi.org/10.5194/piahs-382-213-2020